Bionic Mechanical Analysis of Dragonfly Wings: The Feasibility of Mesh Combination to Improve Structural Stiffness

Yangyang Wei[1], Huidi Guo[1], Siyi Zhang[1], Jingyuan Li[1], Yihan Wang[2] and Chajuan Liu [1,*]

[1]*Architecture and Design College, Nanchang University, Nanchang 330031, China*
[2]*College of Urban Construction, Jiangxi Normal University, Nanchang 330031, China*
E-mail: chajuanliu@126.com
[*]*Corresponding Author*

Received 12 July 2022; Accepted 14 November 2022;
Publication 06 February 2023

Abstract

The nodes of the object will show different degrees of deformation and displacement or even damage over time. The mesh structure is flexible and different mesh shapes and arrangements will affect the structural stiffness of the object. The unique structure of dragonfly wing veins allows the dragonfly to withstand pressures several times higher than itself and to fly freely. This study is based on dragonfly wing bionics to disassemble the structure of dragonfly wing vein geometry. And it aims to investigate the deflection under different geometries and three-dimensional spatial structures by using the drawing software Auto CAD to draw dragonfly sample graphics, the finite element software Hyper mesh to build the model and the solver OptiStruct to analyze the structure of wrinkling, arching deflection, z-direction maximum displacement, y-direction maximum rotation angle, combined displacement test under the different loads. The results show that: (1) The dragonfly wing

European Journal of Computational Mechanics, Vol. 31_4, 459–504.
doi: 10.13052/ejcm2642-2085.3142

vein mesh structure can enhance the stiffness under load. (2) In contrast, the displacement deformation of quadrilateral and combined hexagonal is smaller. (3) The structural stiffness of quadrilateral hexagon is enhanced as the height of wrinkling and arching increases. (4) The improvement of grid deflection with membrane structure is better than that without membrane structure. According to the above experimental results, the quadrilateral wrinkling and hexagonal arching structure has a significant improvement on the load bearing and deflection of the mesh, and has the potential to make structural optimization of the mesh series products, which is suitable for practical application and promotion.

Keywords: Dragonfly wing, vein mesh, stiffness, finite element simulation, mesh structure.

1 Introduction

Inadequate stiffness is one of the reasons for the deformation and damage of many structures, and the deflection of the structure of an object becomes larger with time and pressure from various sources. Although the grid structure has many rods and complex forces, it has the advantages of strong space spanning ability, light weight, integrity, and excellent seismic resistance [1]. Although the grid structure has many advantages, but due to the long life cycle, variable loads including external influences and the existence of substandard material quality, etc., often over time, part of the structure will have various defects [2]. The generation and development of defects such as bending of rods, loosening of nodes, and loosening of bolts will affect the quality of the grid structure to varying degrees [3]. Many deviations in the geometry of rods and nodes and deviations in the surface of the mesh structure, grid structure, and mesh shell structure will have a greater impact on the internal forces and overall stability of the mesh shell, while when the vector height increases, it also increases the unnecessary building space and increases the consumption of building materials and energy [4]. According to the Law of the People's Republic of China on Energy Conservation promulgated by the 10th National People's Congress, the text states that "conservation of resources is the basic state policy of our country" [5], so it is important to continuously optimize the design of the stiffness of the structure, and the reasonable distribution arrangement of the structure can improve the stiffness of the structure. From the biological point of view, the simulation of the mesh structure of dragonfly wings may be a valuable solution.

Dragonflies are known as the "kings of flight" due to their unique wing geometry, material properties, and three-dimensional spatial structure, which enable them to perform a series of difficult flight actions at high speeds and 3600 free flight rotations [6, 7]. In addition to their high manoeuvrability, dragonflies also have an extreme flight endurance. The biologists have observed a thin winged dragonfly capable of crossing the Pacific Ocean [8, 9]. Dragonflies appeared 320 million years ago, and after billions of years, the structure of dragonflies themselves has evolved. And their special body structure deserves further exploration. The unique vein structure of dragonfly wings is also an important reason why dragonflies are able to fly freely at high pressures and mechanics. The wings of dragonflies have a streamlined shape which can mitigate a great deal of wind resistance[10]. And they are covered with longitudinal and transverse wing veins that form a mesh like pattern in the macroscopic state, at the same time the longitudinal veins are decreasing in their tube size and concave convex peaks along the direction of wing tip in a regular pattern, and the mesh is denser near the trailing edge of the wings and the wing tip, which can greatly reduce inertia and relieves stress on the wing tip [11, 12]. Microscopic observation shows that dragonfly wings are not a flat surface, but a three-dimensional structure in space, with a folded shape near the wing root and an archlike structure at the wing tip [13, 14]. It has been studied that the three-dimensional structure of dragonfly wings could improve the forces on the wings and maintain wing stability [15]. Dragonfly wings are made up of a transparent and thin membrane structure, and it has been found that a few microns thick wing membrane contains three layers [16, 17] and the surface of the membrane is covered with a waxlike substance, which allows the structure of dragonfly wings to further enhance the stiffness of the wing veins under loading forces, and also has properties such as self-cleaning and fatigue resistance [18, 19]. Recent developments in bionics have made dragonflies an important object of study for researchers and have given a strong impetus to various aspects of research.

The excellent flight characteristics of dragonflies enable the wings to support various loads during flight. Chao Liu studied the wing microstructure of dragonfly Sphenge pentana, which showed that the dragonfly forewing model has good aerodynamic characteristics and provides a novel bionic concept basis [20]. Nathan Shumway recorded the data of dragonfly analysis of upright and inverted straight flight, and conducted modelling and simulation. It was found that wing deformation of dragonfly plays an important role in the force of wing in the up and down stroke, and the aerodynamic efficiency of deformed wing is higher than that of rigid wing [21]. Zhihui Zhang

studied the rigid veins of dragonfly wings and compared the sample fracture process, and concluded that dragonfly ribs were more rigid [22]. Guanting Su described a method for measuring the maximum force generation of free flying animals and concluded that the maximum performance of dragonfly wings can increase the load [23]. Rudolf J studied the relationship between dragonfly wing structure and accumulated damage from the perspective of fracture mechanics and found that dragonfly wing has special damage tolerance, and crack termination, deflection and bifurcation are the mechanisms to improve wing fracture resistance [24]. Therefore, the solution can be found from dragonfly wing structure by increasing mesh stiffness.

Finite element analysis software is a modern calculation method developed based on structural mechanics analysis, which can solve continuity problems such as fluid mechanics. Heleen Fehervary used finite element software to model and compare mechanical data such as stress, displacement and reaction force of fiberrein forced hyperplastic materials, and concluded that elastic materials can become ideal material models at different levels of complexity [25]. Kumar, D used finite element software to conduct modelling experiments and calculations on the dragonfly biomimetic micro air vehicle, and developed the biomimetic wing with a frequency close to its natural counterpart [26]. Dan Hou used a three-dimensional finite element model to simulate the dynamic deformation behaviour of the dragonfly's front wing. Considering the torsional deformation of the wing, the finite element software simulation concluded that the deformation mechanism of dragonfly's wing played an important role in the design of flexible flapping wing [27]. Xu F used finite element software to extract the excellent structural features of dragonfly veins to design bionic car doors, and the results showed that doors with bionic reinforcement had higher resistance to deformation and vibration [28]. In conclusion, the finite element software was used to simulate and analyze the stiffness of dragonfly wing.

For the mesh structure, its structure is just like the macroscopic form of dragonfly wings. Use the dragonfly wing vein mesh to improve the stiffness of the mesh structure is the focus of our research. We used finite element software to model the dragonfly wings. Then we split and generalized the dragonfly wings and calculated the stiffness of the structure and the deflection under arching for different load conditions and different wrinkle heights by observing and comparing the maximum displacement in z-direction, maximum turning angle in y-direction and combined displacement values of different mesh shapes. The optimum wrinkle height and arch height were obtained by continuous comparison, which was expected to improve the

compressive performance of the mesh structure. The deflections and loads of structures with and without membrane structures of different shapes and heights were analysed and extrapolated through both model building and testing. The effects of wrinkle height on structural stiffness, arch height on structural stiffness, wing membrane on structural stiffness and density of the mesh on structural stiffness were explored in four aspects. And the specific applications and related materials of the mesh structure are to be investigated in subsequent studies.

2 Materials and Methods

In order to study the interaction between the main and full veins in the dragonfly wing mesh vein, the dragonfly wing veins in the dragonfly sample Figure 1 were modelled in 3D by using the finite element analysis software OptiStruct to perform 3D numerical simulations, which in turn led to displacement and corner analysis of the main and full veins of the dragonfly wings. The created models were divided into three main categories.

2.1 Dragonfly wing Bionic Model Building

The models of dragonfly hind wings, main and secondary veins represented the real dragonfly structure, and the most basic geometric structural objects were analyzed from the dragonfly planar mesh for the tests of stiffness under different loads. Considering the accuracy of the experimental results and the characteristics of the finite element software that the simpler the model the more accurate the values, the dragonfly hind wings were selected for static analysis in Figure 2.

Figure 1 The picture of dragonfly sample.

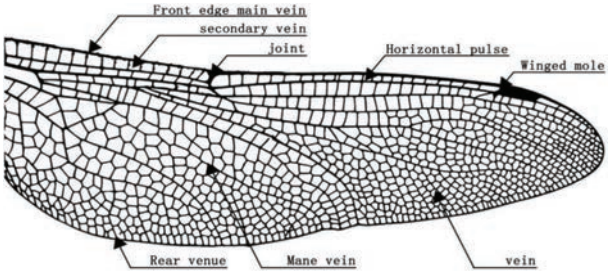

Figure 2 The picture of the right hind wing of the dragonfly after detailed identification.

We observed the dragonfly samples with a microscope and measured the wing diameter, area, outer diameter of the wing vein tube, wall thickness, dragonfly mass, etc. In order to simulate the force deformation of dragonfly wings in real flight, we applied displacement constraints at the wing root and calculated the maximum lift force required for dragonfly wings to fly. Then we simulated and analyzed the cantilever mesh structure. Dragonfly wings are thinwalled space structure. They deform with the increase of external load and have a strong geometric nonlinearity [29]. So when using the finite element software in Figure 3 to analyze the dragonfly vein, the dragonfly wing membrane should consider the effect of geometric nonlinearity. And we used 3 node nonlinear isoparametric beam element beam 189 to simulate the wing vein, as far as possible to restore the deformation of the simulated wing vein in the force.

The Euler Bernoulli beam theory is established based on the flat section assumption that the plane perpendicular to the longitudinal principal axis remains flat and perpendicular to the principal axis before and after beam bending, and only considering the bending deformation. This theory is applicable to beam mechanical analysis. The control equation of the beam element is shown in equation

$$\frac{d^2}{dx^2}\left(EI\frac{d^2v}{d^2}\right) = -w(x) \tag{1}$$

In this context: E is the modulus of elasticity. I is the moment of inertia of the section. W(x) is the distributed force acting on the beam. v is the transverse displacement of the beam, which is the deflection. And x is the longitudinal coordinate.

The beam 189 is a three-dimensional quadratic (3 node) beam element with six or seven degrees of freedom at each node. The element is based on

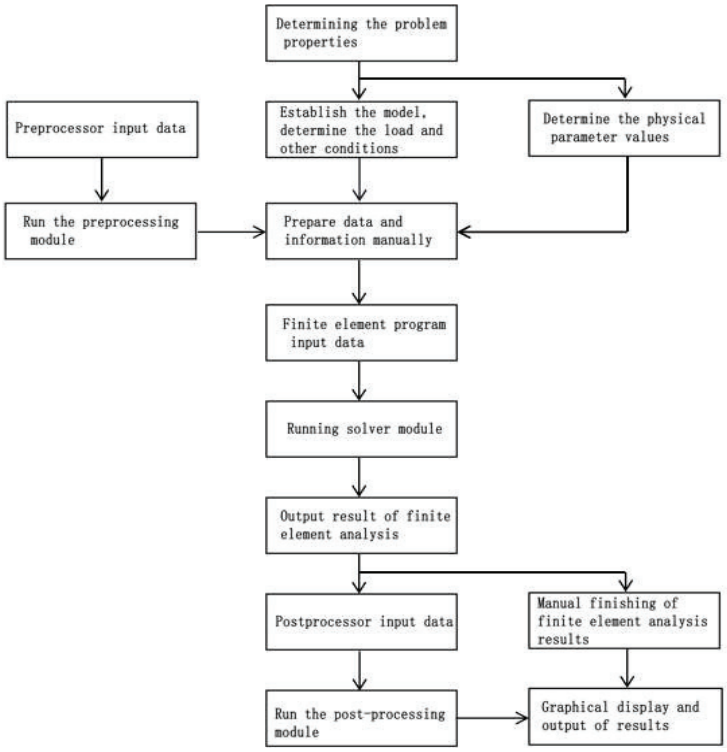

Figure 3 The analysis flow of finite element software.

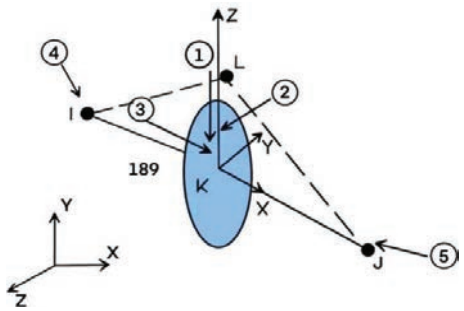

Figure 4 The schematic diagram of the beam189 element.

the structural theory of Temuco, which is suitable for analyzing beam structures ranging from slender to moderately thick and short, and for analyzing linear, largeangle rotation or nonlinear largestrain problems. The schematic diagram of the element is shown in Figure 4.

2.1.1 Grid model building

The morphological simplification of the primary and secondary veins of dragonflies was carried out by microscopic observation of the dragonfly primary and secondary vein meshes. From Figure 5, it was found that the basic geometry of the primary vein structure of dragonfly wings was mostly a quadrilateral cantilever mesh structure, while the secondary veins were mostly triangular, with a combination of pentagonal and hexagonal cantilever meshes, which were called wing chambers [30, 31]. Dragonfly longitudinal veins intertwine with transverse veins to enclose a dense geometric shape [32]. Dragonfly wing veins are divided into convex and concave veins, and the longitudinal veins of dragonfly wings are arranged in strict order of convexity and concavity from the wing root to the wing tip, with the peak of the longitudinal veins becoming progressively less convex and the size of the wing vein tube becoming thinner [33].

Preliminary observations showed that the upper part near the wing root was mostly composed of quadrilateral lattices, while the lower part had more pentagonal lattices and more hexagonal lattices were in the wing tip direction. Microscopic observation of the size of the dragonfly wing veins revealed that the main longitudinal veins of the wings were relatively thick, with the anterior and subanterior marginal veins being the thickest, also known as wing beams. It has been found that dragonflies are able to regulate their energy and stress in response to changes in their flight environment so that they experience minimal drag in flight, and this unique structure of dragonfly wings stems from the fact that dragonfly wings are composed mainly of wing veins and wing membranes [34]. And the wing membranes covered the entire wing veins of the dragonfly and played a protective role.

With the above conclusions to establish the basic geometry finite element model, considering the small mesh of dragonfly wings, we extracted the geometry from it to model with regular ordering. Two dimensional models, orthoquadrilateral and staggered quadrilateral, were established as shown in Figure 6.

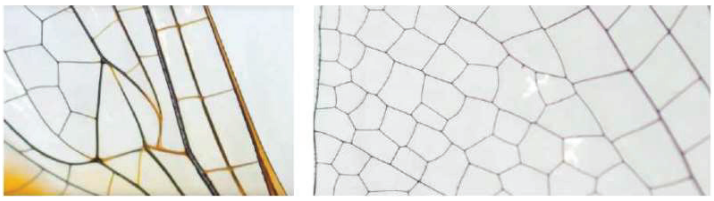

Figure 5 The structure of dragonfly wings magnified one hundred times.

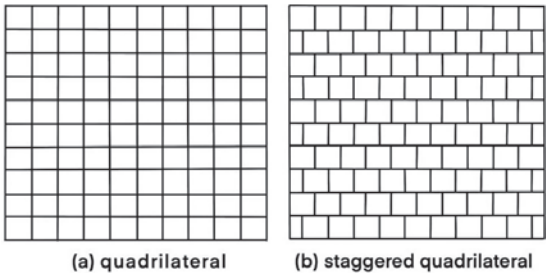

Figure 6 The geometry of the main vein mesh splitting.

According to the actual dimensions of the dragonfly sample, the ortho-quadrilateral cell lengths were taken: a = 20 dmm and b = 15 dmm, which were ordered in a mesh with an outer frame of 200 dm × 150 dmm for analysis. Further considering the special nonlinear structure of dragonfly wings, the wing veins were simulated by using a three-node beam element beam 189, and the elastic modulus was taken as E1 = 3.8 Gpa = 3.8 × 1011 bN/mm^2 in the model according to the Young's modulus in the dragonfly transverse veins, and the Poisson's ratio of the veins was u1 = 0.25, and the density were 2.86 × 104 mg/dmm^3. To further study the influence of the wing membrane on the stiffness, the 8 node isoparametric curved shell element shell was used to simulate the dragonfly wing membrane, and the TriboInderter in situ nanomechanical test system was used to obtain the material properties [28]. The elastic model was E2 = 1.5 Gpa = 1.5 × 1011 bN/dmm^2. The Poisson's ratio was u2 = 0.25. The shell thickness was h = 0.02 dmm, and the finite element model was established.

The eight-node isoparametric shell element shell93 theory is that Shell93 is an eight-node isoparametric shell element, which can simulate a more ideal shell with curved boundary, and it is more applied in the problems of large strain, stress stiffening and large deformation, and it can accurately restore the mass of dragonfly wing membrane [36]. All the membranes in this paper were simulated by the shell93 element. Each node of this element had 6 degrees of freedom, which means it moved and rotated along the direction of coordinate points X, Y and Z [37]. The schematic diagram of the element is shown in Figure 7.

In the dragonfly wing mesh structure, the mesh structure in the secondary vein is more complex, most of them are hexagonal with larger area and combined hexagonal (three, five, hexagonal) [38]. At the leading edge and root of the dragonfly wings, the grid shows a lateral distribution, in the middle of the wings the distribution direction of the grid appears at a clear angle to

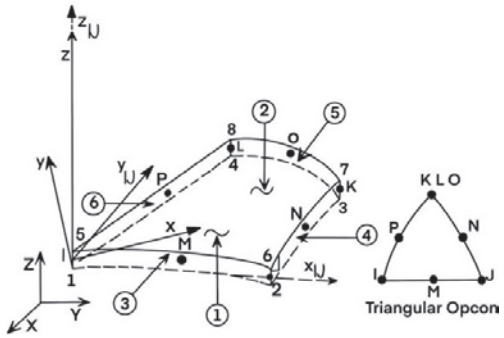

Figure 7 The geometrical relationship of shell93 elements.

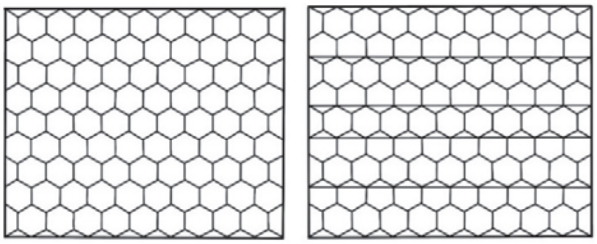

Figure 8 The splitting geometry of secondary vein mesh.

the horizontal direction, and at the trailing edge of the wings part of the grid distribution direction is perpendicular to the wing spreading direction [39]. For the hexagonal with more nodes, the displacement deformation is more likely to occur under the force load compared to the quadrilateral mesh [40], so the positive hexagonal and combined hexagonal mesh were established to simulate the effect of the geometry in the secondary vein on the stiffness as shown in Figure 8. According to the actual size of the dragonfly sample, the hexagonal element side length a = 10 dmm was taken and ordered in the mesh outer frame size: 173 dmm × 140 dmm. The same value of elastic modulus quadrilateral mesh model was E1 = 3.8 × 1011 bN/mm^2. The Poisson's ratio of the vein was u1 = 0.25. The beam outer diameter was R = 1 dmm. The wall thickness was taken as r = 0.25 dmm. The wing film elastic model was E2 = 1.5 × 1011 bN/dmm^2. The poisson's ratio was u2 = 0.25. The shell thickness was h = 0.02 dmm, and the finite element model was established for mechanical analysis.

Among them, the cylinder shell wall thickness was calculated by the formula [31],

$$\mathrm{S} = \mathrm{PDi}/(2 * [\delta\ \mathrm{t}] * ¢\mathrm{P}) + \mathrm{C} \tag{2}$$

P is the pressure (kg/cm^2), D is the diameter (mm).

2.2 The Establishment of Dragonfly Wing Bionic 3D Mesh Model

In bionomics, a large number of scholars have collected a lot of data on the cross-section, shape, and structure of dragonfly wings, and found that the shape of dragonfly wing cross-section shows wrinkles along the wing root, and the thickness of the entire wrinkled form on the wing also has subtle differences [42]. The wrinkled structure is a special structure unique to dragonfly wings among many insects that evolved after billions of years of superiority and inferiority [43]. It has been found that the pleated structure has been shown to improve the bending stiffness and structural deflection of the structure while significantly reducing the weight of dragonflies and maintaining their stability during flight [44, 45]. Dragonfly wing span direction lattices show mostly three, five, and six deformations, and it was found that the dragonfly polygonal lattices are not planar but show arched bridge curvature, further increasing the stiffness of the dragonfly wings and serving as a material saving function [46]. A 3D wrinkled and arched model of the basic geometric structure the dragonfly wing mesh was extracted from the dragonfly wing mesh. The unique quadrilateral wrinkled and hexagonal arched structure of the dragonfly wing was derived by observing the 3D structure of the dragonfly wing, and the professor Li Zhongxue from Zhejiang University did a related study on the cross-sectional microstructure of the dragonfly wing as shown in Figure 9. It has been demonstrated that under microscopic observation, the dragonfly wing was not a smooth plane, but performed in different positions In order to further analyse the aerodynamic properties of dragonfly wings, a model has been developed as shown in

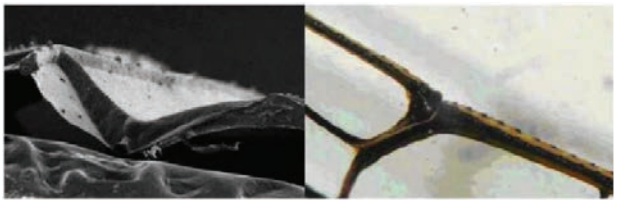

Figure 9 The microstructure of dragonfly wings.

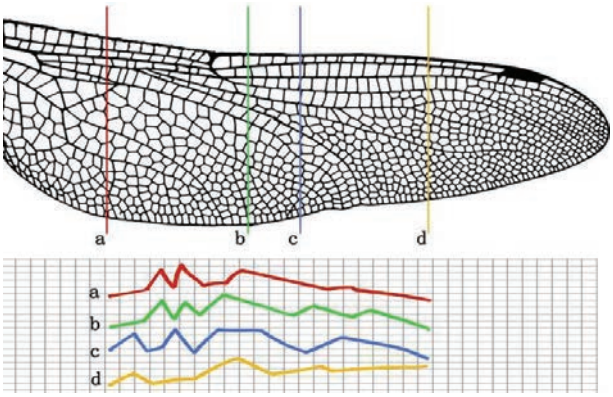

Figure 10 Four cross-sections of the dragonfly's hind wings.

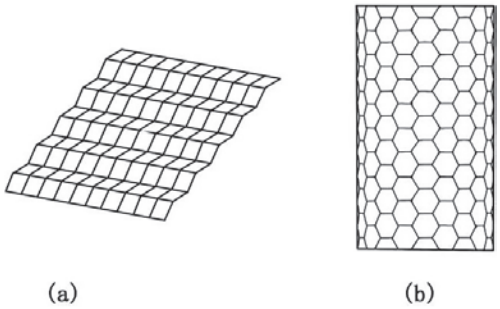

Figure 11 A picture of the quadrilateral wrinklearch model. (a) is the model of a quadrilateral wrinkling height of 5 dmm; (b) is the model of a hexagonal span ratio of 1/3.

Figure 10, We can see that the three-dimensional structure of cross-section a near the wing root first shows wrinkling and then continues to decline; cross-sections b and c near the middle of the wing show lower wrinkling than cross-section a and decline more; cross-section d near the tip of the wing shows significantly less wrinkling and declines more gently, thus confirming that the dragonfly wing is indeed a threedimensional structure with wrinkling and arching and the height of wrinkling decreases with the root of the wing towards the wing.

In order to further analyse the aerodynamic aspects of the dragonfly wings, a relevant model was developed. Based on the abovementioned planar quadrilateral mesh model, the relevant parameters were retained and the quadrilateral structure with different wrinkling heights and the hexagonal structure with different arches were added to the model as shown in Figure 11.

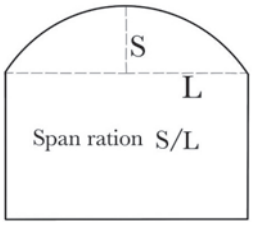

Figure 12 The schematic diagram of the risespan ratio calculation.

The theory of rises pan ratio: The calculated the rise S and the calculated span ratio L in an arch bridge (S/L) is called the degree of rise, which is an important indicator of the force characteristics of an arch bridge. It has been shown that the wingtip of the dragonfly was arched in the direction of the wingtip, so the net rise and the net span diameter of different rises pan ratio need to be calculated when modelling. The schematic diagram of the rises pan ratio calculation is shown in Figure 12.

2.3 Experiments with Loads

For the model of cantilever beam mesh, the load test is a "special test" in the category of beam structure testing [47], which includes "static load test" and "dynamic load test" [48]. The static load test is the test located on the foundation, which refers to the determination of the deformation modulus of an object under natural conditions through a certain pressure test [49, 50]. It can check the design and construction quality of the beam structure and obtain the actual load carrying capacity of the beam structure. Measurements of dragonfly wing mesh loads were divided into nonuniform and uniform loads. Considering the deformation and stresses of the wings when subjected to uniform loads or wingtip forces [51], it examined the uniform loads, distributed loads, static forces, and concentrated forces perpendicular to the wing surface to obtain the stiffness of the dragonfly wings, respectively. When the wing made a simple two-dimensional swing, it can be considered as a rigid swinging cantilever beam. So the force load was loaded linearly along the wing root toward the wing with the equation $Px = cx$ [52]. Based on our main study of the mesh stiffness, we determined that it was most appropriate to use the uniform load, which is the force uniformly distributed on the structure. The equation for calculating the bending moment of the uniform load is simply considered as $M = (q*x2)/2$ and x is the length of the uniform load [53].

2.4 Material Characteristics and Simulation Details of Load Experiment

2.4.1 The properties of materials

Our previous mesh analysis modeling of dragonfly wings showed that the wing veins were separated from the most basic geometry by observation and modeled in three dimensions. To further simulate the complex mechanics of dragonfly wings in a realistic way, we would build a more accurate finite element model by analyzing the dragonfly wing veins and wing membranes according to the dragonfly wing veins.

The dragonfly wing vein is a tube-shaped hollow structure with different cross-sections at different locations [54]. The hollow structure not only effectively reduces the weight of the dragonfly wing but also relieves the alternating stresses generated during flight. And the wall of the dragonfly wing vein is a composite structure and the laminated structure can ensure that the wing vein will resist fatigue cracks in flight and withstand greater torsional deformation to some extent [55]. Therefore, we used the simplicity but accuracy of the finite element software to model and analyze the hollow tube with an inner diameter of 1 dmm and an outer diameter of 1.4 dmm. The thickness of the wing membrane decreased along the wing root toward the wing chord, tightly wrapping the wing vein, and the flexible wrapping method could reduce the generation of cracks in the vibrating wings [56, 57]. The tensile properties and displacement of the wing membrane provided enlightening ideas for the subsequent design topology optimization.

It is also important to note that we used the same material properties for all the established finite element models, and this modeling allowed us to maximize the reproduction of the realistic force effects on the dragonfly wings.

2.4.2 The detailed setup of the load experiment

The article applies a force load to the three groups of models and makes a deflection analysis and comparative study of the mechanical response of the three groups of models. We must compare them under the same load to get the most accurate data. Observation of the dynamics showed that the dragonfly wings were subjected to air forces and inertial forces generated by their own accelerated motion in flight, and the wings were deformed to different degrees [58]. The finite element software OptiStruct obtained displacement and stress clouds by applying different loads, so it was important for us to apply a uniform load to the model simulation process. Because the dragonfly

wing root is connected to the main body of the dragonfly, we selected a fixed displacement loading method for the experiment. In all models, displacement constraints were applied near the wing root, and the dragonfly wing vein loading was selected as the minimum lift force required for dragonfly flight, $q = mg/(A1 + A2)$, where mg was the total mass of the dragonfly, A1 was the front wing area, and A2 was the hind wing area. To study the coordination performance of the dragonfly under structural deformation of the wing veins, a concentrated force F was applied at the primary and secondary veins, respectively. And the size of F was taken from the mass of the dragonfly itself, while the uniform load applied by the geometric mesh model combined with the minimum lift force for dragonfly wing flight was taken as $F = 10000\ bN \times (1, 2, 3, 4, 5, 6, 7, 8, 9)$. We performed the analysis of displacement, turning angle and deflection for each model under the conditions of each load. The deflection analysis was a necessary step to ensure the effect of the dragonfly wings on the stiffness.

3 Results

In this study of the geometric mesh stiffness structure of dragonfly wings, three finite element models were set up, which were the finite element model based on the dragonfly sample, the planar model of the dragonfly wing mesh split geometry and the 3D structural mesh finite element model. By observing the turning angles, displacements, and stresses of the wings and meshes through different loads, the results contained four parts. Firstly, a load comparison of displacement values and calculation of deflections at 15 nodes for the main and full veins of the finite element wing model of the dragonfly sample. Secondly, a comparative study based on quadrilateral and staggered quadrilateral meshes split from the wings according to the 3D wrinkle pattern of the dragonfly wings. Finally, the stiffness of the arched orthohexagon and the combined hexagon were compared under different heights of arching. And the above experimental analysis led to the conclusions.

3.1 The Structural Analysis of the Dragonfly Wing Vein

The shape and dimensions of the samples were observed and measured under a microscope, and the wings were split into main and full veins. A set of original sample dimensions were taken and plotted as a planar gt software Hyper mesh to build the model. And the dragonfly finite element model was built as show in Figure 13.

3.2 The Stiffness Analysis of the Dragonfly Wing Vein

In order to accurately simulate the forces and deformations of the dragonfly wings, mechanical analysis of the cantilevered mesh structure was carried out by applying displacement constraints at the wing roots of the model. The same uniform load was applied at the main and full veins, and the uniform load was taken as the minimum lift force of 895.15 bN/dmm^2 required for the dragonfly to fly on its own [6]. The deflection, displacement and deformation values for the two models were studied under the uniform load. Figure 14 shows the deflection analysis, y-directional displacement and x-directional turning angle for the main and full veins respectively at the uniform load of 895.15 bN/dmm^2.

To further observe the deformation pattern of the structure, 15 points were taken at each of the same positions of the dragonfly's main vein and full vein, as shown in Figure 13. To further observe the deflection of the nodes at different positions, The experimental results are shown in Table 1.

By studying the displacement and turning angle data of the primary and secondary veins under the uniform load of 895.15 bN/dmm^2, it was determined that the displacement magnitudes of the nodes at different locations were different. In the following, the deformation displacement of the dragonfly wing vein structure under the action of the concentrated force was further determined. The same displacement constraint was applied at the wing root of the dragonfly, and a concentrated force F in the z-axis direction was applied at the wing tip of the primary and secondary veins. F was taken as 159.5 mg of the dragonfly's self-weight, and the displacement values and maximum turning angles of the primary and total veins under the action of the concentrated force were observed. Figure 15 is the graph of y-directional displacement and x-directional turning angles of the primary and total veins under the effect of the concentrated force.

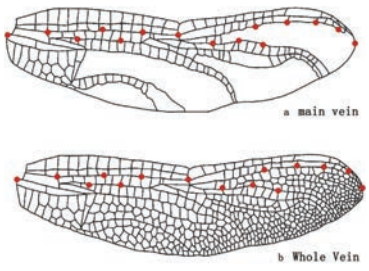

Figure 13 The finite element model of the dragonfly wing and the 15 observatioints. (a) is the main vein of the dragonfly. (b) is the whole vein of the dragonfly.

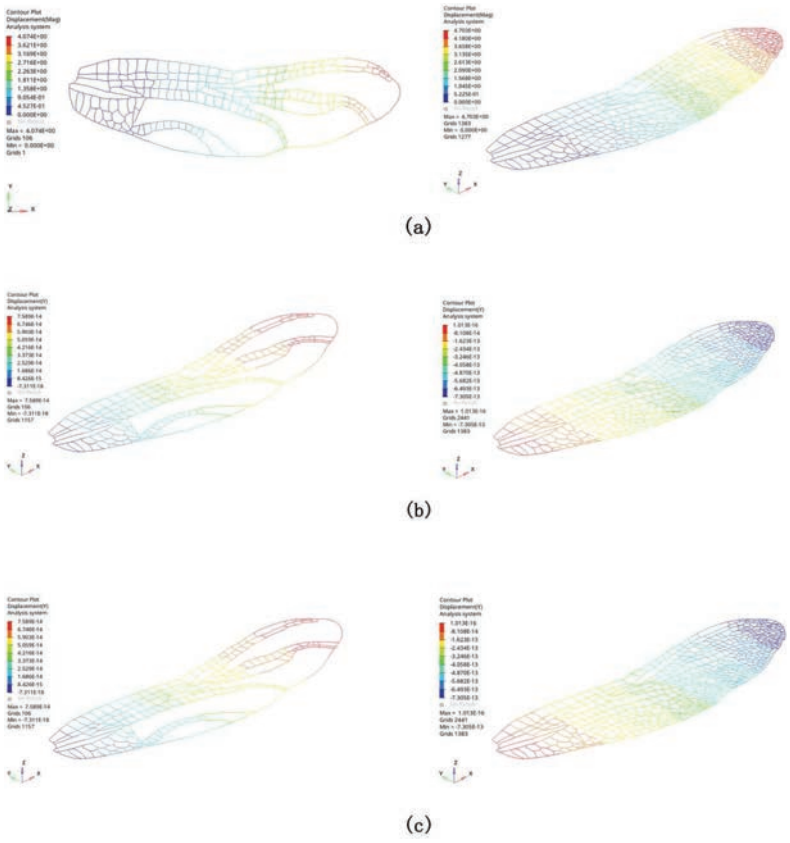

Figure 14 The comparative deflection analysis graphs for the main and full veins of the dragonfly. (a) is the analytical graph of the deflection for the main and full veins under uniform load. (b) is the graph of the y-directional displacement for the main and full veins under uniform load and (c) is the graph of the x-directional turning angle for the main and full veins under uniform load.

Under the effect of concentrated force F, the deflection of the nodes under different positions was observed at 15 nodes in the same position of the main vein and the whole vein of the dragonfly, which is shown in Figure 13. And the experimental results are shown in Table 2.

3.3 Wing Bionic Mesh Mechanical Analysis

In order to further understand whether there is a correlation between the vein shape and stiffness of dragonfly wings, four basic geometric cantilever

Table 1 The deflection values of the main and full veins under uniform load (in dmm)

Observation Point Number	Main Vein	Full Pulse
1	0	0
2	0.09	0.113
3	0.286	0.376
4	0.508	0.626
5	0.689	0.86
6	0.957	1.157
7	1.429	1.702
8	1.911	2.3
9	2.287	2.789
10	2.55	2.964
11	2.681	3.23
12	3.076	3.552
13	3.491	4.071
14	3.815	4.39
15	4.074	4.703

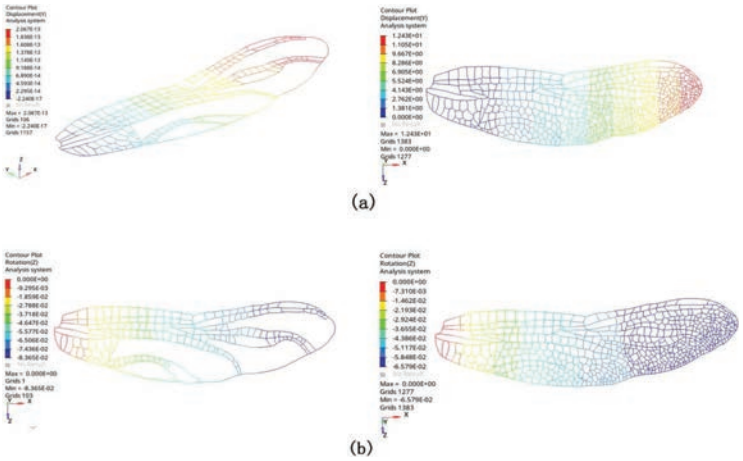

Figure 15 The deflection graphs of the main and secondary veins under the concentrated force at 159.5 mg. (a) shows the y-directional displacement graphs of the main and total veins under the concentrated force. (b) shows the x-directional turning angle graphs of the main and total veins under the concentrated force at the wing tip.

mesh structures were isolated from the dragonfly wing structure. They were positive quadrilateral mesh, staggered quadrilateral mesh, positive hexagonal mesh, triple, quintuple and hexagonal mesh, which were experimented under wrinkle and arch and different loads, and the results were observed.

Table 2 The deflection values of the main and full veins under the action of the concentrated force (in dmm)

Observation Point Number	Main Vein	Whole Pulse
1	0	0
2	0.233	0.245
3	0.756	0.832
4	1.383	1.42
5	1.901	1.961
6	2.733	2.699
7	4.254	4.134
8	5.884	5.642
9	7.238	6.965
10	8.253	7.498
11	8.695	8.178
12	10.284	9.174
13	11.925	10.515
14	13.291	11.576
15	14.235	12.431

We applied displacement constraints at the wing roots and took the quadrilateral (a) and the staggered quadrilateral (b) of Figure 6. Combining the lift force as F = 10000bN $\times$ (1.2.3.4.5.6.7.8.9.10) for the dragonfly flight state and taking F = 7 $\times$ 104 bN for the uniform load, we observed the y-directional displacement graphs and x-directional turning angle graphs for the quadrilateral (a) and staggered quadrilateral (b) at a wrinkle height of 0 dmm, as shown in Figure 16.

The dragonfly wing is a threedimensional structure with a wrinkled structure along the wing tip at the wing root, The dragonfly wing is a three-dimensional structure with a folded structure along the wing tip at the wing root, so a displacement constraint was applied at the wing root to observe the y-directional displacement graphs and x-directional turning angle graphs of the positive quadrilateral mesh and staggered quadrilateral mesh at a wrinkle height of 4 dmm and the uniform load of F = 7 $\times$ 104 bN, as shown in Figure 17.

3.4 Bionic Fin Film Shell Stiffness Analysis

Displacement constraints were applied at the wing roots and the quadrilateral (a) and staggered quadrilateral (b) of Figure 6 were taken to observe the change in stiffness with and without the shell at the same wrinkle heights of 0,

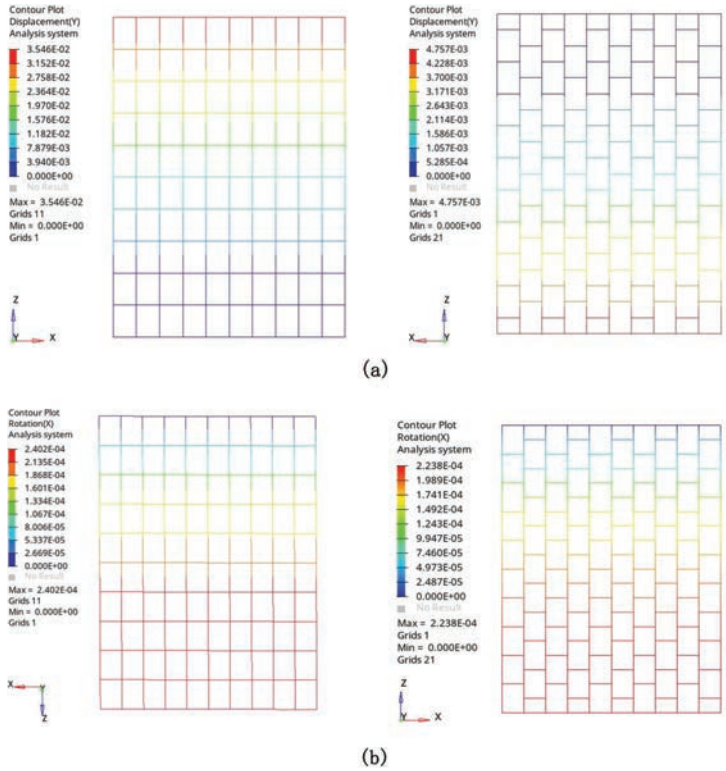

Figure 16 The displacement and turning angle graphs for the quadrilateral and staggered quadrilateral at a wrinkle height of 0 dmm. (a) is y-directional displacement graph for quadrilateral and staggered quadrilateral (at a wrinkle height of 0 dmm). (b) is x-directional corner graph for quadrilateral and staggered quadrilateral (at a wrinkle height of 0 dmm).

4, 8 and 10 dmm and the same load of F = 10,000 bN × (1.2.3.4.5.6.7.8.9.10), under different loads, respectively.

We observed the y-directional displacement graphs and x-directional turning angle graphs of the membrane quadrilateral and the membrane staggered quadrilateral at a wrinkle height of 4dmm and under the uniform load of F = 7 × 104 bN as shown in Figure 18 and compared their stiffness.

To further observe whether the membrane quadrilateral and staggered quadrilateral increased in stiffness with the change in wrinkle height, a new model was created. We observed the y-directional displacement and x-directional turning angle graphs of the membranous quadrilateral and staggered quadrilateral for a wrinkle height at 0 and under a uniform load of F = 7 × 104 bN, as shown in Figure 19.

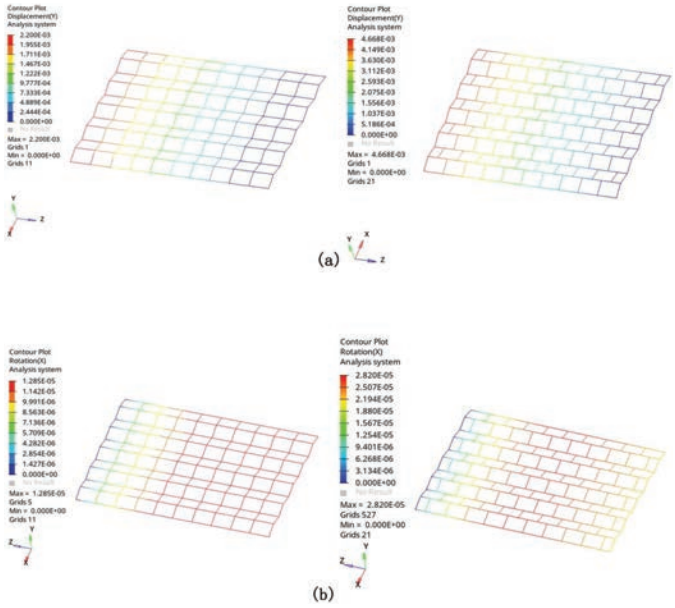

Figure 17 The maximum turning angle graphs and displacement graphs for the quadrilateral and staggered quadrilateral meshes for a wrinkle height at 4 dmm. Figure 17 shows the maximum turning angle graphs and displacement graphs for the quadrilateral and staggered quadrilateral meshes for a wrinkle height at 4 dmm. (a) is y-directional displacement isogram for the quadrilateral and staggered quadrilateral (at a wrinkle height of 4 dmm). (b) is x-directional corner plot for the quadrilateral and staggered quadrilateral (at a wrinkle height of 4 dmm).

The x-axis displacement graph, y-axis displacement graph, z-directional displacement graph and y-directional turning angle graph for the membrane quadrilateral and the staggered quadrilateral at a wrinkle height of 4 dmm under a uniform load $F = 7 \times 104$ bN, as shown in Figure 20.

We further observed and compared the maximum displacement values of the quadrilateral with and without membrane, and the staggered quadrilateral with and without membrane under the uniform load of $F = 1 \times 104$ bN and $F = 8 \times 104$ bN at the wrinkle height of 4 dmm, as shown in Figure 21.

3.5 Mechanical Analysis of Wing Bionic Arch Mesh

In studying the dragonfly wing mesh, we found that the dragonfly wings appeared wrinkled at the wing root and arched at the wing tip, and the arc of the secondary vein arch was the largest in the threedimensional structure

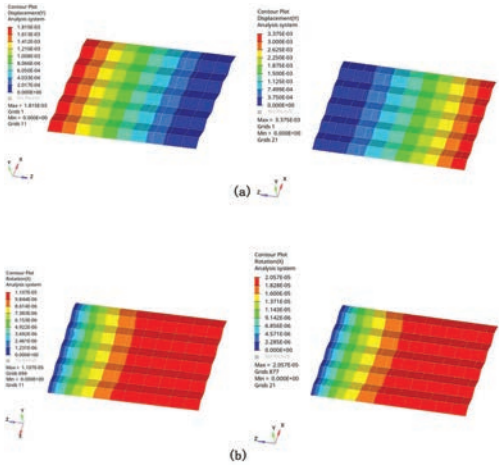

Figure 18 The y-directional turning angle graphs and x-directional displacement graphs for the quadrilateral with membrane and the staggered quadrilateral with membrane mesh under the uniform load of F = 7 × 104 bN and at the wrinkle height of four. Among them, (a) is the y-directional displacement isogram for the quadrilateral with membrane and the staggered quadrilateral with membrane (wrinkle of 4 dmm). (b) is the x-directional turning angle graph of the quadrilateral with membrane and the staggered quadrilateral with membrane (wrinkle of 4 dmm).

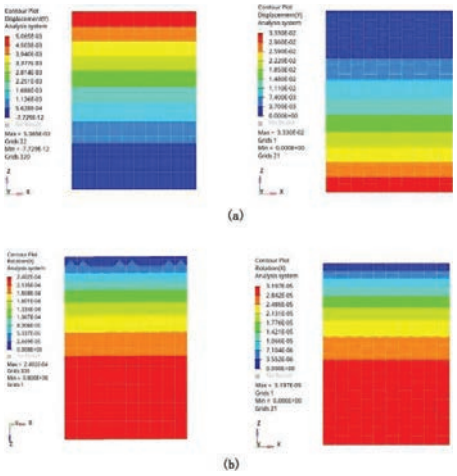

Figure 19 The y-directional displacement graphs and the x-directional turning angle graphs for the membrane quadrilateral and the membrane staggered quadrilateral under the same load at a wrinkle height of 0dmm. Among them, (a) is the maximum y-directional displacement of the membranous quadrilateral and the staggered quadrilateral. (b) is the maximum x-directional turning angle of the membranous quadrilateral and the staggered quadrilateral with membranes.

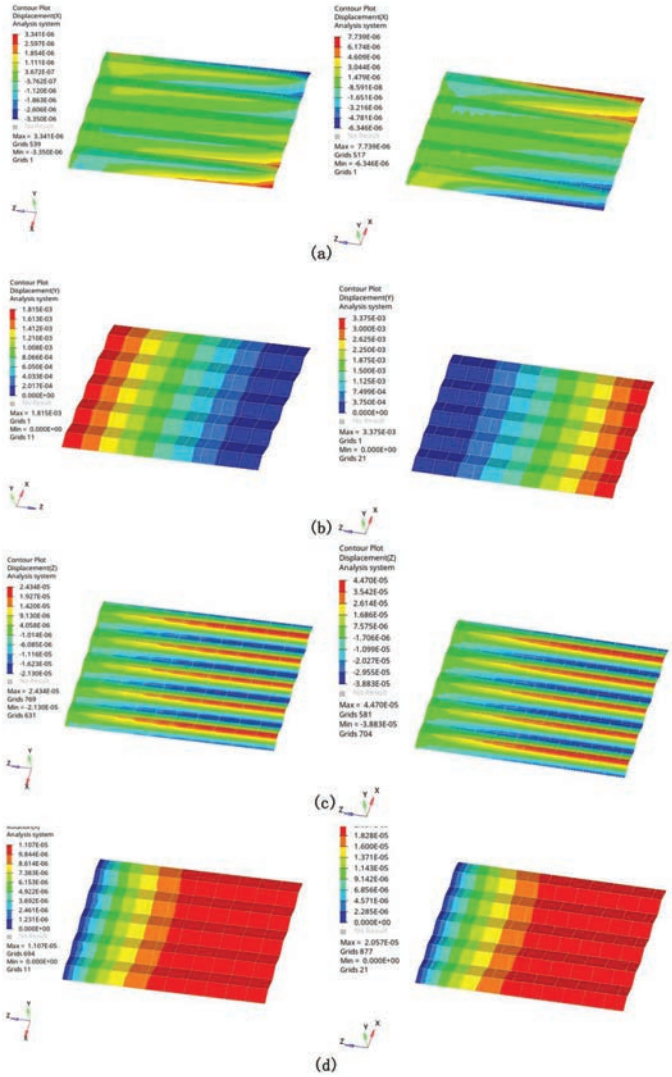

Figure 20 The displacement graphs and turning angle graphs for the membrane quadrilateral and the staggered quadrilateral under the same load at a wrinkle height of 4 dmm. (a) is the maximum x-directional displacement of the quadrilateral with membrane and the staggered quadrilateral. (b) is the maximum y-directional displacement of the quadrilateral with membrane and the staggered quadrilateral with membrane. (c) is the maximum z-directional displacement of the quadrilateral with membrane and the staggered quadrilateral with membrane. (d) is the x-directional turning angle graph of the quadrilateral with membrane and the staggered quadrilateral with membrane.

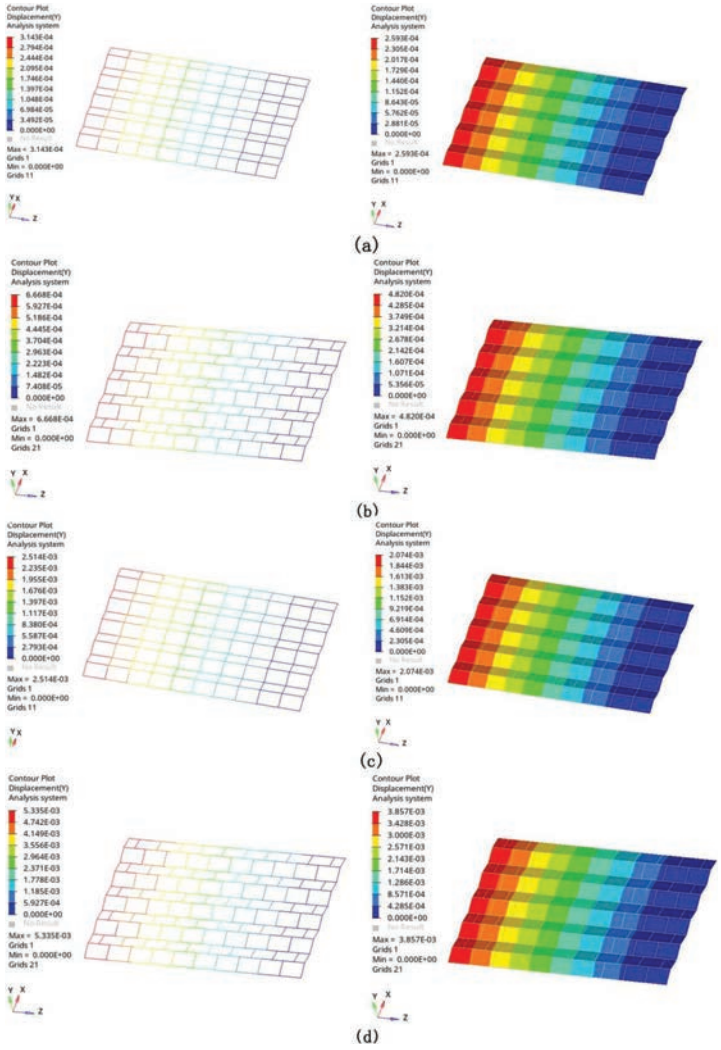

Figure 21 The displacement graphs of the quadrilateral with and without the membrane, and the staggered quadrilateral with and without the membrane under different loads and at a wrinkle height of 4 dmm. Among them, (a) is the maximum displacement in y-direction under the load of F = 1 × 104 bN for quadrilateral with and without the membrane. (b) is the maximum displacement in y-direction under the load of F = 1 × 104 bN for staggered quadrilateral with and without the membrane. (c) is the maximum displacement in y-direction under the load of F = 8 × 104 bN for quadrilateral with and without the membrane. (d) is the maximum displacement in y-direction under the load of F = 8 × 104 bN for staggered quadrilateral with and without the membrane.

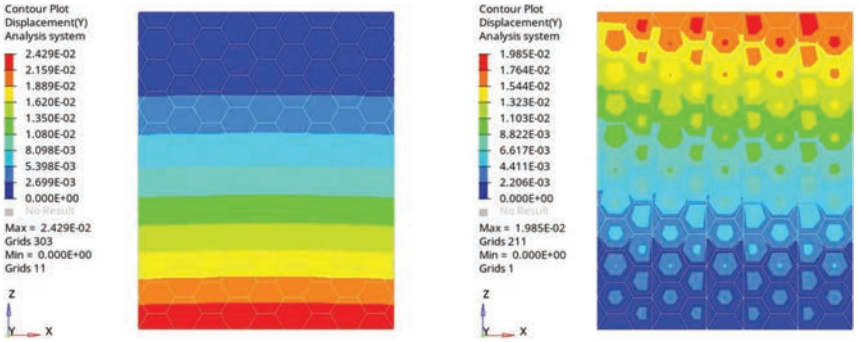

Figure 22 The displacement graphs of the positive hexagon with membrane and the combined hexagon under the same load and at the risespan ratio of 0. (a) is the graph of maximum displacement in the y-direction of the hexagon with the membrane. (b) is the graph of maximum displacement in the y-direction of the combined hexagon with the membrane.

of the dragonfly. After the analysis, we classified the dragonfly wing subvein mesh shapes as hexagonal and (tri, penta, and hexa) sided. To verify whether the arch of the dragonfly wing has an effect on the structural stiffness, we further established a finite element model for analysis as shown in Figure 8. We performed static analysis experiments with membrane hexagon and combined hexagon under the load of F, and observed the stiffness variation of the two hexagonal meshes under different loads. The displacement constraint was applied at the wing root and the y4-directional displacement graphs of the membranous hexagon and the combined membranous hexagonal mesh under a uniform load of $F = 7 \times 104$ bN were observed in Figure 22.

After observing the arching of the threedimensional structure of Dragonfly subvein, therefore, the maximum directional displacement graphs of the membranous hexagonal mesh and the combined mesh under the uniform load of $F = 7 \times 104$ bN and at the risespan ratios of 0, 1/9, 1/6, and 1/3 were observed, as shown in Figure 23.

We further observed the directional displacement graphs, directional displacement graphs, and directional displacement graphs of the membranous hexagonal mesh and the combined hexagonal mesh for the risespan ratio of 1/3 under a uniform load of $F = 7 \times 104$ bN, as shown in Figure 24.

To ensure more realistic simulation experimental data, the maximum displacement values of z-directional displacement graphs, x-directional displacement graphs, y-directional displacement graphs, and combined displacement graphs of membranous hexagon and combined hexagon with a risespan

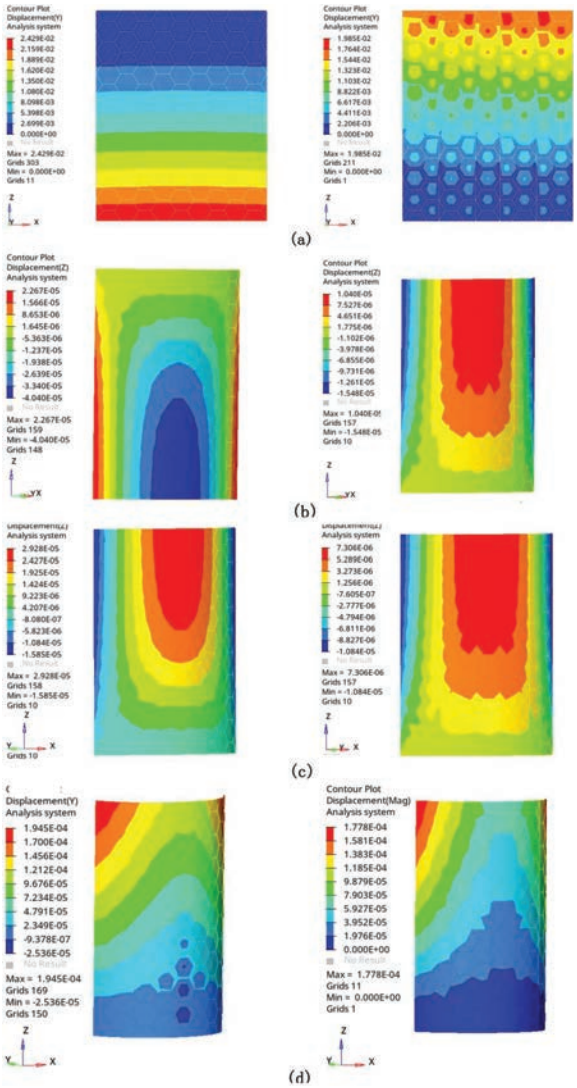

Figure 23 The displacement graphs of the membranous orthohexagon and the combined hexagon under the same load and at different risespan ratios. Among them, (a) is the graph of the maximum displacement in y-direction of the membranous hexagon and staggered hexagon for the risespan ratio of 0. (b) is the graph of the maximum displacement of the membranous hexagon and staggered hexagon for the risespan ratio of 1/9. (c) is the graph of the maximum displacement in y-direction of the membranous hexagon and staggered hexagon for the risespan ratio of 1/6. And (d) is the graph of the maximum displacement of the membranous hexagon and staggered hexagon for the risespan ratio of 1/3.

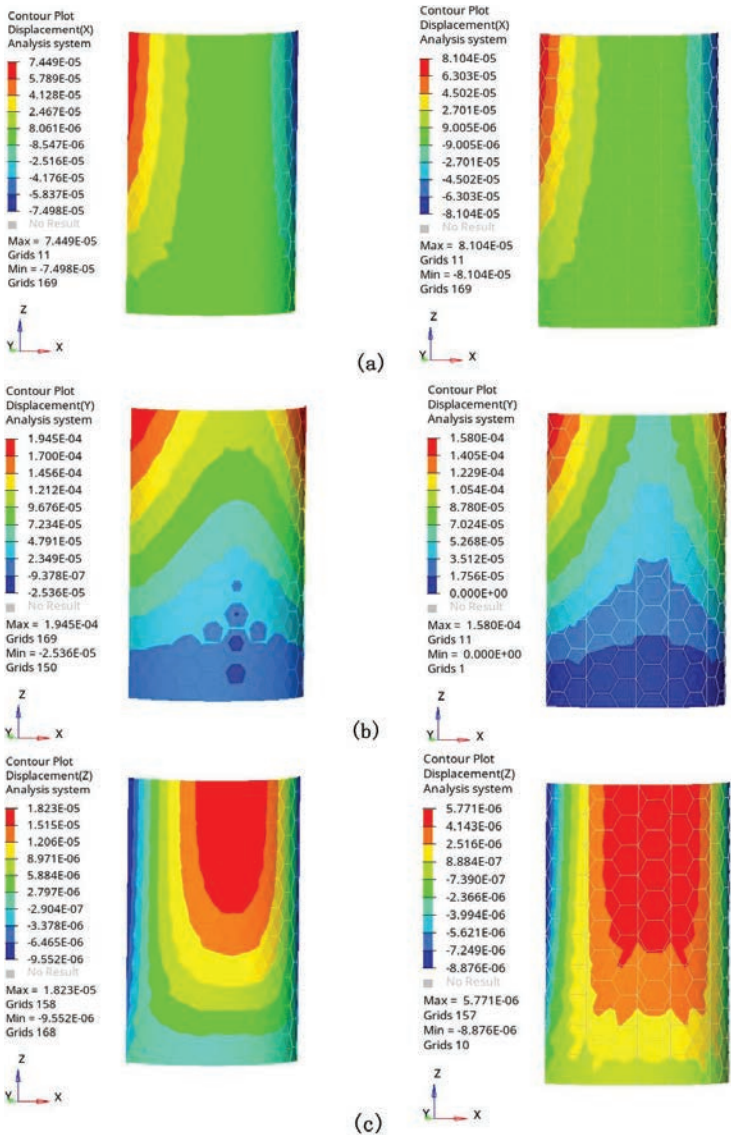

Figure 24 The displacement graphs of a orthohexagon with the membrane and a combined hexagon under the same load and at a risespan ratio of 1/3. (a) is the x-direction maximum displacement graphs of the membranous hexagon and staggered hexagon with the risespan ratio of 1/3. (b) is the y-direction maximum displacement graphs of the membranous hexagon and staggered hexagon with the risespan ratio of 1/3. (c) is the z-direction maximum displacement graphs of the membranous hexagon and staggered hexagon with the risespan ratio of 1/3.

Table 3 The displacement values of the hexagon under uniform load

Load/ 10^4bN	x Direction/ dmm	y Direction/ dmm	z Direction/ dmm	Combined Displacement/dmm
1	1.06E^{05}	2.78E^{05}	2.06E^{06}	2.98E^{05}
2	2.13E^{05}	5.56E^{05}	5.21E^{06}	5.96E^{05}
3	3.19E^{05}	8.33E^{05}	7.81E^{06}	8.94E^{05}
4	4.26E^{05}	1.11E^{04}	1.04E^{05}	1.19E^{04}
5	5.32E^{05}	1.39E^{04}	1.30E^{05}	1.49E^{04}
6	6.39E^{05}	1.67E^{04}	1.56E^{05}	1.79E^{04}
7	7.45E^{05}	1.95E^{04}	1.82E^{05}	2.09E^{04}
8	8.51E^{05}	2.22E^{04}	2.08E^{05}	2.38E^{04}
9	9.58E^{05}	2.50E^{04}	2.34E^{05}	2.68E^{04}
10	1.06E^{04}	2.78E^{04}	2.61E^{05}	2.98E^{04}

Table 4 The displacement values of the combined hexagon under uniform load

Load/ 10^4bN	x Direction/ dmm	y Direction/ dmm	z Direction/ dmm	Combined Displacement/dmm
1	1.16E^{05}	2.26E^{05}	8.24E^{07}	2.54E^{05}
2	2.32E^{05}	4.25E^{05}	1.65E^{06}	5.08E^{05}
3	3.47E^{05}	6.77E^{05}	2.47E^{06}	7.62E^{05}
4	4.63E^{05}	9.03E^{05}	3.30E^{06}	1.02E^{04}
5	5.79E^{05}	1.13E^{04}	4.12E^{06}	1.27E^{04}
6	6.95E^{05}	1.36E^{04}	4.95E^{06}	1.52E^{04}
7	8.10E^{05}	1.58E^{04}	5.77E^{06}	1.78E^{04}
8	9.26E^{05}	1.81E^{04}	6.60E^{06}	2.03E^{04}
9	1.04E^{04}	2.03E^{04}	7.42E^{06}	2.29E^{04}
10	1.16E^{04}	2.26E^{04}	8.24E^{06}	2.54E^{04}

ratio of 1/3 and under different loads were observed, and each displacement value is shown in Tables 3 and 4.

4 Discussion

In order to study how the stiffness of the meshed forms can be increased, we used dragonfly wings as our main object of study and quadrilateral and hexagonal mesh structures as a maximization strategy to increase the stiffness of the permutations. In this thesis, we present experimental data on the deflection of dragonfly main and full veins, quadrilateral and combined quadrilateral wrinkles, and hexagonal and combined hexagonal arches under different uniform loads and concentrated forces. And based on the available

data, a feasible approach to improve the stiffness of the lattice structures is proposed.

4.1 The Effect of the Mesh Wrinkle Forms

Based on known conclusions and observations of dragonfly samples, we established a finite element model of the dragonfly wing for loading experiments. Firstly, the stiffness of the main and secondary veins of the dragonfly was tested. According to the graphs of deflection analysis and graphs of displacement turning angle under the load of 895.15 bN/dmm^2 in Figure 14, it could be seen that the maximum deflection of the main and full veins were all at the wing tip, increasing along the wing root towards the wing tip. In the graph of displacement, the maximum displacement of the main vein is 7.589E14 dmm and the full vein is 1.013E16 dmm. And the turning angle of the model of the main vein and the full vein around the xaxis under the uniform load also increases gradually along the direction of the wing span. The maximum turning angle value of the main vein is 7.589E14 dmm, and the full vein turning angle value is 1.013E16 dmm. From Table 1 we learn that the values of the fifteen nodes uniformly distributed on the wings also differ significantly under a uniform load. The deformation pattern of the dragonfly wings is the same in both cases, and the overall deformation of the main vein is the largest under the same load, and the deflection of each corresponding node is slightly lower than the deflection applied on the fullvein model, further indicating that the full vein has a greater influence on the deflection of the main frame, and the bending stiffness of the main vein pair is larger and has stronger stability and bearing capacity.

Figure 25 shows the deflection distribution curves of the fifteen nodes in the wing under uniform load, from which we can see that the difference in deflection values between the main and full veins is not significant under the same load and position, so it is clear that the secondary veins have little effect on the stiffness of the dragonfly veins and that the main veins have greater stiffness and stability. The displacement value of the main vein under uniform load was greater than that of the full vein. It can be seen in Figure 15 that the y-directional displacement value of the main vein is 2.067E13 dmm and that of the main vein is 2.737E15 dmm under the concentrated force of the wing tip, and that the turning angle value of the main vein is greater than that of the full vein in the x-directional from the graphs of the turning angle. The maximum deflection of both models occurs at the wing tip position, Figure 26 shows the curves of Table 2 in which we can see that the values of

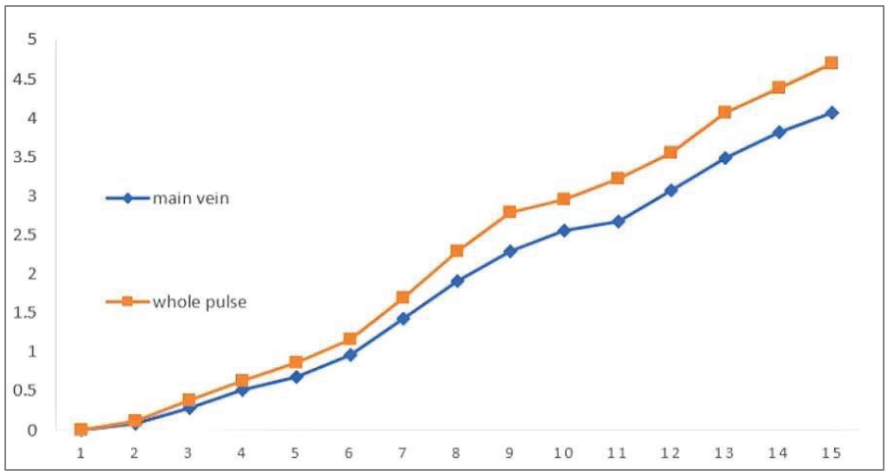

Figure 25 The deflection distribution curves of the main vein and the full vein of the dragonfly under the uniform load.

both models are deformed significantly compared to the values under uniform load, but both show an overall deformation trend with 15 characteristic nodes of deflection values increasing along the wing root toward the wing tip. The maximum stresses of both the main vein and the full vein are at the wing root, and the stresses in the middle and wing tip are relatively small, which reflects the superior performance of the dragonfly wings in terms of overall compressive deformation resistance. From Figure 26, it can be seen that the two curves of the main vein and the full vein under the action of the concentrated force near the wing root basically overlap, but gradually separate along the wing tip direction. Although the concentrated force acts at the wing tip, the grid transfers the force borne at the wing tip to the wing root fixation under the action of bending moment, which reflects the superior performance of the dragonfly wing structure in terms of overall deformation coordination under the action of external force. The deformation direction and size of each position on the dragonfly wing veins are not the same, but all of them undergo overall deformation, and the deformation at the junction of the primary and secondary veins is coordinated under the action of load, which jointly improves the stiffness of the overall wing, so it can be seen that the dragonfly wing does have an excellent stiffness structure.

Based on the quadrilateral and combined quadrilateral cantilever meshes separated from the main veins of the dragonfly wings, we compared the

deflection values of the two sets of models. Figure 16 shows that in the planar mesh, the quadrilateral mesh y-direction displacement value is 3.546E02 dmm, and the staggered quadrilateral mesh is 4.757E03 dmm, which can be seen that the comparison of deflection values is not significant. According to the threedimensional characteristics of dragonfly wings, the dragonfly wings form a wrinkled structure at the wing root. In Figure 17, it can be seen that the wrinkle height of four under uniform load, the quadrilateral wrinkle mesh stiffness is significantly increased. The value of displacement is 2.200E03 dmm, and the value of turning angle is 1.285E05 dmm. The value of wrinkled displacement of staggered quadrilateral is 4.688E03 dmm, and the value of turning angle is 2.820E05 dmm. It has been known that the dragonfly wing membrane enhances stiffness. From Figure 18, it can be seen that in the wrinkled quadrilateral with membrane and the staggered quadrilateral under the same load, the value of y-directional displacement of the positive quadrilateral mesh is 1.815E03 dmm, which is 0.38503 dmm less compared to no membrane, and the value of x-directional turning angle is 1.7806 dmm less compared to no membrane. The value of y-directional displacement of the staggered quadrilateral is 1.31303 dmm less compared to no membrane, and the value of x-directional turning angle is 7.6306 dmm less than one has no membrane. The deflection and corner values with film are smaller than those of the mesh without film, Figure 19 shows that the deflection of the quadrilateral mesh with membrane is reduced by 3.0304 dmm and the deflection of the staggered quadrilateral mesh with membrane is reduced by 207 dmm compared to the nonmembrane quadrilateral mesh at a wrinkle height of 0 dmm. Figure 20 shows that the overall deflection of the quadrilateral mesh is less than that of the staggered quadrilateral mesh for the same wrinkle height and uniform load. Under the z-direction uniform load, the highest part of the fold is elongated and the deepest part of the fold is compressed. Under the y-direction uniform load, the spatial model is no longer deformed along the y-direction, and a small amount of deformation is also generated along the x-direction and z-direction. Figure 21 shows that for different uniform loads and the same wrinkle height, compared with the quadrilateral mesh with membrane and the quadrilateral mesh without membrane, the maximum displacement value in y-direction is smaller than that of the quadrilateral mesh without membrane, the displacement value of the staggered quadrilateral mesh with membrane is smaller than that of the staggered quadrilateral mesh without membrane, and the displacement of the staggered quadrilateral mesh with membrane is larger

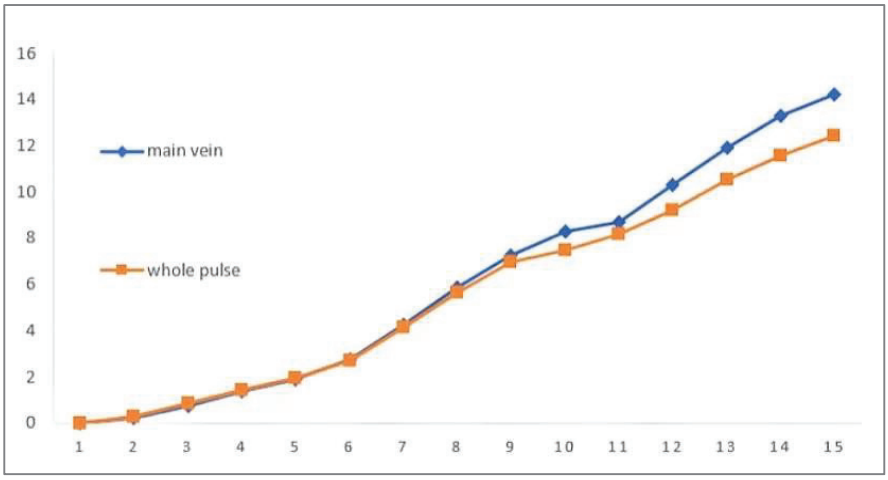

Figure 26 Deflection distribution curves of the main vein and full vein of the dragonfly under concentrated force.

than that of the quadrilateral mesh with membrane, The deflection value increases with the enhancement of the load.

From the above analysis, it can be obtained that in the planar model, the influence of membrane and no membrane on the stiffness of the structure is not significant, but with the wrinkling of the mesh, the stiffness of the positive quadrilateral mesh with membrane is always greater than that of the staggered quadrilateral mesh structure under the same load, and the stiffness increases with the increase of the wrinkling height. It can be seen that in the threedimensional structure of dragonfly wings, the wrinkling of the wings makes the stiffness of the grid structure enhanced, the wing membrane has a certain influence on the stiffness of the structure, and the shell in the grid interacts with the grid to enhance the overall stiffness of the grid, and as the wrinkling height increases, the shell has a stronger role in coordinating the deformation of the overall structure of the grid.

4.2 The Role of the Mesh Arched Structure

According to the known literature about the arch of dragonfly wing secondary veins threedimensional structure, we separated the orthohexagonal and (three, five, six) sided mesh forms from the dragonfly wing geometry for compar. According to the known literature about the arch of dragonfly wing secondary veins threedimensional structure, we separated the orthohexagonal and (three,

five, six) sided mesh forms from the dragonfly wing geometry for comparison. In Figure 22, It can be seen that in the planar state, the orthohexagonal with membrane y-directional displacement value is 2.429E02 dmm, and the combined hexagonal displacement value is 1.985E02 dmm. According to the comparison of the stiffness of different arch heights based on the dragonfly wing arch, as shown in Figure 23, with different risespan ratios, the lowest value of y-directional displacement of the positive hexagon with membrane is 1.945E04 dmm for the risespan ratio of 1/3, and the lowest value of displacement of the combined hexagon with membrane is 1.778E04 dmm for the risespan ratio of 1/3. The stiffness of the combined hexagonal mesh is greater than that of the orthohexagonal mesh for the risespan ratio of 1/3. Under the same uniform load, the deflection of the arching grid is much lower than the maximum deflection value of the planar grid, and the deflection of both the hexagonal grid with membrane and the combined hexagonal grid with membrane decrease significantly with the increase of the vectortospan ratio, which proves that the higher the height of the arching, the smaller the structural deflection of the grid. Figure 23 shows the further observation of the displacement data of the hexagonal mesh with membrane and the combined hexagonal mesh at the risespan ratio of 1/3. According to this figure, it can be seen that the combined hexagonal has a smaller value of 1.246E5 dmm compared to the positive hexagonal in the y-direction displacement, and the mesh has the largest displacement along the y-direction. e further observation of the displacement data of the hexagonal mesh with membrane and the combined hexagonal mesh at the risespan ratio of 1/3. According to this figure, it can be seen that the combined hexagonal has a smaller value of 1.246E5 dmm compared to the positive hexagonal in the y-direction displacement, and the mesh has the largest displacement along the y-direction.

Figures 27 and 28 show the maximum displacement trends of different directional axes of the cantilever mesh model for risespan ratio of 1/3 in Tables 3 and 4, respectively. It can be seen in the figure that the value of the combined displacement in the mesh is the largest and the value of the z-directional displacement is the smallest under the load, and the overall displacement value of the combined hexagonal mesh is smaller than that of the orthohexagonal mesh. From the above data, it is clear that the deflection value of the combined hexagon with membrane is always smaller than the deflection value of the positive hexagon with membrane under the same load and vectortospan ratio. The surface tension of the membrane in the starting hexagonal grid increases with the increase of external load, and the grid has a significant improvement of the structural resistance to deformation

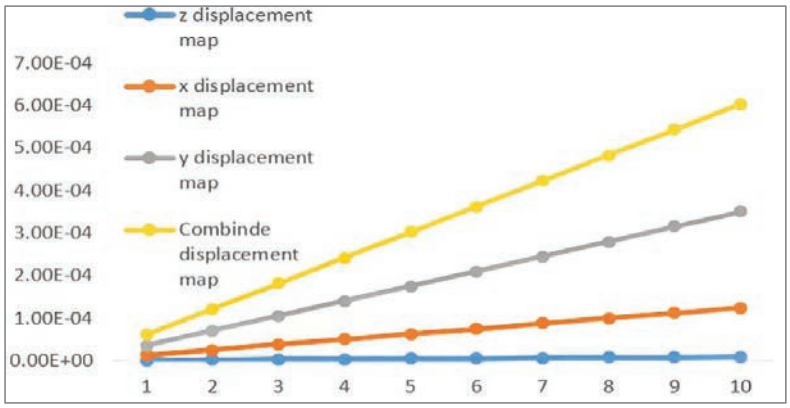

Figure 27 The trend of axes in each direction of the hexagonal mesh with membrane under the uniform load.

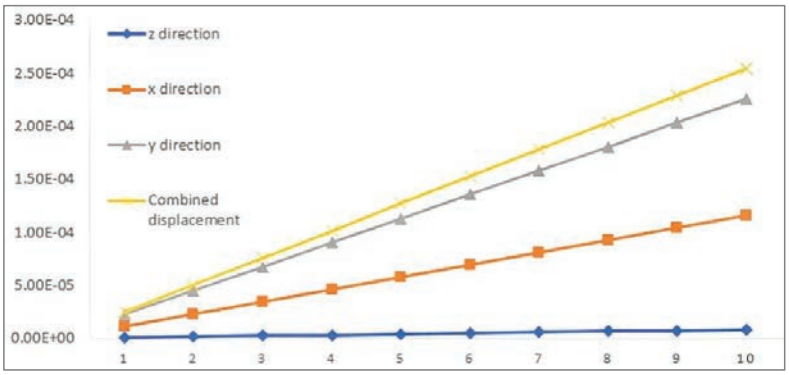

Figure 28 The trend of each directional axis of the combined hexagonal mesh with membrane under the uniform load.

under the action of the surface tension of the shell. Under the action of the surface tension, the load acting on the fin vein is dispersed to each point along the fin membrane, which alleviates the deformation along the load direction, improves the overall deformation coordination ability of the structure, and enhances the stiffness of the grid structure. Through the above subinformation, the density of the combined hexagonal grid is greater than that of the orthohexagonal grid, and the increase of the combined grid density increases the loadbearing structure and enhances the resistance to deformation, indicating that the grid density can also affect the stiffness of the structure, and the greater the density the greater the stiffness.

5 Conclusions and Outlook

As the most widely used structure, the mesh structure must study the development law of its stiffness to ensure its reliability in structural engineering, and scholars at home and abroad have conducted a lot of research and achieved a series of research results. The geometric mesh decomposed from dragonfly wings was subjected to finite element modeling to compare the deflection under different loads, and the mesh model was analyzed according to the threedimensional characteristics of dragonfly wings with the aim of improving the stiffness of the mesh structure. In this study, the deflection analysis of the geometric cantilever beam mesh derived from the dragonfly wing analysis was carried out under different loads, and the deflection comparison was carried out by adding the shell to this mesh according to the overlay structure on the dragonfly wing mesh, and the displacement and deflection of the quadrilateral mesh and the staggered quadrilateral mesh under different wrinkle heights and different uniform loads according to the characteristics of the structure of the dragonfly wing with wrinkles at the threedimensional wing roots and arches at the wing tips analysis. For the displacement and deflection analysis of hexagonal meshes and combined hexagons under different lifttospan ratios and different uniform loads, as can be seen from the finite element software simulations. By simulating the main vein and the full vein on the wings of the dragonfly samples and applying uniform load through the finite element modeling to simulate the lift required for the real flight of the dragonfly, the comparison shows that the stiffness of the main vein of the dragonfly is less than that of the full vein.

Through the above experimental data, we further add 15 observation nodes to the main full vein of the dragonfly and find that the deflection and turning angle of the main full vein gradually increase along the wing root toward the wing tip, and the maximum deflection appears at the wing tip. Under the same load, the edge shape of the node at the main vein is the smallest, and the edge shape at the secondary vein increases, which further indicates that the main vein, as the main frame of the whole wing, has stronger stability and pressurebearing performance. The overall comparison of the main and full veins reveals that the combination of the main and secondary veins with each other can significantly improve the overall stiffness and reduce the displacement range of the structure. Based on the above study, the analysis of the concentrated force at the wing tip of the dragonfly shows that both the main vein and the full vein produce overall deformation under the concentrated force, and the mesh transmits the force from the

wing tip to the wing root under the concentrated force, which reflects the superior coordination performance of the dragonfly wing structure. Based on the observation of the dragonfly sample, the wing split into quadrilateral and staggered quadrilateral for load analysis shows that the stiffness of quadrilateral mesh is greater than that of staggered quadrilateral mesh. The stiffness of quadrilateral and staggered quadrilateral meshes further increases with the increase of wrinkle height based on the threedimensional structure of dragonfly wing, and the stiffness of quadrilateral and staggered quadrilateral meshes increases with the increase of wrinkle height under the same load. The deflection and displacement values and turning angle values of the quadrilateral and staggered quadrilateral meshes with membrane are smaller than the corresponding deflection, displacement and turning angle values without membrane at the same wrinkle height and under the same load. The stiffness of the quadrilateral mesh with membrane and the staggered quadrilateral mesh with membrane is always greater than that of the staggered quadrilateral mesh with membrane at the same wrinkle height and under different loads. According to the threedimensional structure of dragonfly secondary vein splitting hexagonal mesh and combined hexagonal mesh, the combined hexagonal with membrane mesh is better than the orthohexagonal with membrane mesh in the planar mesh state. The stiffness of hexagonal mesh with membrane and combined hexagonal mesh in the arching state increases significantly with the increase of risespan ratio, and the mesh deflection increases with the increase of load. Adding membrane to the hexagonal mesh according to the characteristics of the dragonfly wing membrane, the value of displacement and deformation of the structure decreases significantly under the tension of the membrane. The combination of the mesh and membrane is beneficial to improve the overall performance of the mesh, and the increase of the mesh density further enhances the loadbearing structure. The edge shape of the combined hexagonal mesh is always smaller than that of the positive hexagonal mesh.

This bionic study of dragonfly wing structure using a series of finite element models confirms that the geometry in the dragonfly wings can improve the stiffness of the structure. Due to the unique wing structure of the dragonfly, quadrilateral meshes assume the main stress points of the wings, and quadrilateral wrinkles in different directions can bring different effects, and further investigation is needed on the direction of quadrilateral mesh wrinkles and how to apply them. The unique arch structure of the dragonfly wing makes the load and force range spread further, and the wing tip, which is far from the fixed constraint, transmits the force to the wing root, reducing the

risk of fracture and collapse. The excellent structure of dragonfly wings has important implications for the improvement of mesh structures in architecture and can be further applied to a wide range of engineering aspects inspired by the study of dragonfly wing structures. Possible applications include mesh structure buildings, meshshell structure buildings, etc. There are many types of mesh structures, including cross truss system mesh, triangular cone system mesh, and quadrangular cone system mesh, etc. [59]. The mesh structure is a spatial structure made of multiple rods connected by nodes according to a certain grid form, which has the advantages of high stiffness and good seismic performance, and is mostly used in the roofs of buildings such as stadiums, exhibition halls and stadium canopies [60]. As a high subsuperstationary structure, the mesh structure can better withstand concentrated load, dynamic load and asymmetric load, and has excellent seismic performance [61], however, different mesh structures can cause different degrees of damage to the mesh structure according to the increase of time and various extreme external factors and unexpected conditions such as irresistible forces, and the study of dragonfly wing bionic structure can well solve this problem, extend the life of the mesh The research of dragonfly wing bionic structure can solve this problem well, extend the service life of the structure, increase the stiffness of the structure so that the net frame structure has a stronger earthquake resistance function.

The guardrail belongs to the grid structure in civil engineering, and there are many kinds of guardrails with a wide range of application [62], and some of them need stronger stiffness to ensure safety because of the special environment they are in. Highspeed rail and railroad line guard fence plays a key role for personal property when the train runs at high speed, but due to the distant railroad route, coupled with the uncertainty of the environment in which the guardrail mesh is located, the maintenance and operation cost of the guardrail increases, the quadrilateral wrinkles in the bionic dragonfly wing grid can increase the stiffness of the fence, the hexagonal grid of the arch structure can save materials, use and arc can reduce the sudden injury by 70% The arched structure of hexagonal mesh can save material and reduce sudden damage by 70%, which can optimize the function and stiffness of the fence and its service life to a large extent.

The meshshell structure is a spatial rod system structure similar to the flat mesh frame, with the rod as the basis for the composition of the grid and arranged according to the shell structure of the spatial framework [63]. The meshshell structure also includes singlelayer meshshell structure, prestressed meshshell structure, etc [64]. Meshshell structures have the main

characteristics of both rod and thinshell structures, can span large spans, and their shells contain different materials. In the dragonfly bionic mesh structure, the dragonfly wings are composed of translucent film, which can further enhance the stiffness and tensile and compressive resistance of the steel structure, so that the wings remain stable under unstable loads, and therefore the dragonfly bionic mesh structure can still enhance the stiffness of the shell structure. Dragonfly bionic carport structure makes outstanding contribution to the overall stiffness of grid mesh structure, mesh shell structure, etc. However, due to the limitations of the study, only the structural form of the mesh is discussed in this paper, and the material aspects and practical applications are yet to be further studied.

References

[1] Zhang Q. Research on the construction schedule and cost optimization of grid structure based on BIM and genetic algorithm[C]//Journal of Physics: Conference Series. IOP Publishing, 2021, 1744(2): 022065.

[2] Gasii G M. Structural and design specifics of space grid systems. Science & Technique. 2017, 16(6): 475–484. https://doi.org/10.21122/2227-1031-2017-16-6-475-484

[3] Wei X C, Fan J S, Liu Y F, et al. Automated inspection and monitoring of member deformation in grid structures[J]. Computer-Aided Civil and Infrastructure Engineering, 2022, 37(10): 12771297.

[4] Doan Q H, Lee D. Optimal formation assessment of multilayered ground retrofit with archgrid units considering buckling load factor[J]. International Journal of Steel Structures, 2019, 19(1): 269282.

[5] Lu Li. Energy Saving Law of the People's Republic of China. Safety Technology of Special Equipment, 2022, 04, 36.

[6] Shumway N, Gabryszuk M, Laurence S J. Flapping tandemwing aerodynamics: dragonflies in steady forward flight[C]//2018 AIAA aerospace sciences meeting. 2018: 1290.

[7] Phillips P, Swanson BJ. A genetic analysis of dragonfly population structure. Ecol Evol. 2018 Jun 25;8(14):72067215. doi: 10.1002/ece3.4255. PMID: 30073079; PMCID: PMC6065342.

[8] Ismael S, HE Abdel Aleem S, Abdelaziz A, et al. Optimal harmonic passive filters for power factor correction, harmonic mitigation and electricity bill reduction using dragonfly algorithm[J]. 2019.

[9] Lietz C, Schaber CF, Gorb SN, Rajabi H. The damping and structural properties of dragonfly and damselfly wings during dynamic movement.

Commun Biol. 2021 Jun 15;4(1):737. doi: 10.1038/s42003021022632. PMID: 34131288; PMCID: PMC8206215.

[10] Rajabi H, Gorb S N. How do dragonfly wings work? A brief guide to functional roles of wing structural components[J]. International Journal of Odonatology, 2020, 23(1): 2330.

[11] Swain P K, Dora S P. Experimental and numerical investigation of wing–wing interaction and its effect on aerodynamic force of a robotic dragonfly during hovering and forward flight[J]. Archive of Applied Mechanics, 2021, 91(5): 20392052.

[12] Zhang, S., Ochiai, M., Sunami, Y. et al. Influence of Microstructures on Aerodynamic Characteristics for Dragonfly Winsimg in Gliding Flight. J Bionic Eng 16, 423–431 (2019). doi.org/10.1007/s4223501900343.

[13] Nixon MR, Orr AG, Vukusic P. Wrinkles enhance the diffuse reflection from the dragonfly Rhyothemis resplendens. J R Soc Interface. 2015 Feb 6;12(103):20140749. doi: 10.1098/rsif.2014.0749. PMID: 25540236; PMCID: PMC4305401.

[14] Chitsaz N, Marian R, Chahl J. Experimental method for 3D reconstruction of Odonata wings (methodology and dataset). PLoS One. 2020 Apr 29;15(4):e0232193. doi: 10.1371/journal.pone.0232193. PMID: 32348334; PMCID: PMC7190169.

[15] Au L T K, Phan H V, Park S H, et al. Effect of corrugation on the aerodynamic performance of threedimensional flapping wings[J]. Aerospace Science and Technology, 2020, 105: 106041.

[16] Vahdani A, Darvizeh A, Alitavoli M, et al. Numerical investigation of the material gradient using different stiffness functions by consideration of the graded stiffness of the dragonfly wing membrane[J]. Journal of Science and Technology of Composites, 2021, 8(1): 13071316.

[17] Zhang Z, Zhang L, Yu Z, et al. Insitu mechanical test of dragonfly wing veins and their crack arrest behavior[J]. Micron, 2018, 110: 6772.

[18] Lang X, Song B, Yang W, et al. Effect of Wing Membrane Material on the Aerodynamic Performance of Flexible Flapping Wing[J]. Applied Sciences, 2022, 12(9): 4501.

[19] Chen R Y, Lai C J, Chen Y J, et al. Omnidirectional/Unidirectional AntireflectionSwitchable Structures Inspired by Dragonfly Wings[J]. Journal of Colloid and Interface Science, 2022, 610: 246257.

[20] Liu C, Du R, Li F, Sun J. Bioinspiration of the vein structure of dragonfly wings on its flight characteristics. Microsc Res Tech. 2022 Mar;85(3):829839. doi: 10.1002/jemt.23952. Epub 2021 Sep 28. PMID: 34581475.

[21] Shumway N, Gabryszuk M, Laurence S. The impact of dragonfly wing deformations on aerodynamic performance during forward flight. Bioinspir Biomim. 2020 Feb 7;15(2):026005. doi: 10.1088/17483190/ab597e. PMID: 31747648.

[22] Zhang Z, Zhang L, Yu Z, Liu J, Li X, Liang Y. Insitu mechanical test of dragonfly wing veins and their crack arrest behavior. Micron. 2018 Jul;110:6772. doi: 10.1016/j.micron.2018.05.003. Epub 2018 May 5. PMID: 29753176.

[23] Su G, Dudley R, Pan T, Zheng M, Peng L, Li Q. Maximum aerodynamic force production by the wandering glider dragonfly (Pantala flavescens, Libellulidae). J Exp Biol. 2020 Jul 15;223(Pt 14):jeb218552. doi: 10.1242/jeb.218552. PMID: 32457065.

[24] Rudolf J, Wang L Y, Gorb S N, et al. On the fracture resistance of dragonfly wings[J]. Journal of the Mechanical Behavior of Biomedical Materials, 2019, 99: 127133.

[25] Fehervary H, Maes L, Vastmans J, Kloosterman G, Famaey N. How to implement userdefined fiberreinforced hyperelastic materials in finite element software. J Mech Behav Biomed Mater. 2020 Oct;110:103737. doi: 10.1016/j.jmbbm.2020.103737. Epub 2020 May 5. PMID: 32771879.

[26] Kumar, D., Mohite, P.M. & Kamle, S. Dragonfly Inspired Nanocomposite Flapping Wing for Micro Air Vehicles. J Bionic Eng 16, 894–903 (2019). https://doi.org/10.1007/s4223501901046.

[27] Hou D, Zhong Z. Comparative analysis of deformation behaviors of dragonfly wing under aerodynamic and inertial forces. Comput Biol Med. 2022 Jun;145:105421. doi: 10.1016/j.compbiomed.2022.105421. Epub 2022 Mar 21. PMID: 35366473.

[28] Xu F, Wang J, Hua L. Multiobjective biomimetic optimization design of stiffeners for automotive door based on vein unit of dragonfly wing. Proceedings of the Institution of Mechanical Engineers, Part C: Journal of Mechanical Engineering Science. 2022;236(9):45514564. doi: 10.1177/09544062211053471.

[29] Zhen Wang, Baoguo Li, QuanQuan Luo, Wenli Zhao,Effect of wall roughness by the bionic structure of dragonfly wing on microfluid flow and heat transfer characteristics, International Journal of Heat and Mass Transfer, 2021, ISSN 00179310, doi.org/10.1016/j.ijheatmasstransfer.2021.121201.

[30] Cornelius J K, Opazo T, Schmitz S, et al. Dragonfly–Aerodynamics during Transition to Powered Flight[C]//77th Annual Vertical Flight Society Forum and Technology Display. 2021.

[31] Chu Y J, Ganesan P B, Ali M A. Fluid–structure interaction simulation on flight performance of a dragonfly wing under different pterostigma weights[J]. Journal of Mechanics, 2022, 37: 216229.

[32] Minor A M, Dehm G. Advances in in situ nanomechanical testing[J]. MRS Bulletin, 2019, 44(6): 438442. Lima J P S, Cunha M L, dos Santos E D, et al. Constructal Design for the ultimate buckling stress improvement of stiffened plates submitted to uniaxial compressive load[J]. Engineering Structures, 2020, 203: 109883.

[33] Zhang J, Wang Y, Deng H, Zhao C, Zhang Y, Liang H, Gong X. BioInspired Bianisotropic MagnetoSensitive Elastomers with Excellent Multimodal Transformation. ACS Appl Mater Interfaces. 2022 May 4;14(17):2010120112. doi: 10.1021/acsami.2c03533. Epub 2022 Apr 20. PMID: 35442629.

[34] Wang Y, Ma T, Pei D, et al. Effect of magnetically confined plasma on the fatigue life of a thickwalled cylinder[J]. IEEE Transactions on Plasma Science, 2020, 48(4): 10081015.

[35] Rajabi H, Rezasefat M, Darvizeh A, et al. A comparative study of the effects of constructional elements on the mechanical behaviour of dragonfly wings[J]. Applied Physics A, 2016, 122(1): 113.

[36] Rajabi H, Darvizeh A. Experimental investigations of the functional morphology of dragonfly wings[J]. Chinese Physics B, 2013, 22(8): 088702.

[37] Cheeseman S, Truong V K, Walter V, et al. Interaction of giant unilamellar vesicles with the surface nanostructures on dragonfly wings[J]. Langmuir, 2019, 35(6): 24222430.

[38] Zhang S, Sunami Y, Hashimoto H. Deformation behavior of dragonfly-inspired nodus structured wing in gliding flight through experimental visualization approach[J]. Scientific reports, 2018, 8(1): 17.

[39] Zhao R. Calculation of Internal Force and Deformation of Overlying Soil Corrugated Arch Bridge Based on Plate and Shell Theory[C]//IOP Conference Series: Earth and Environmental Science. IOP Publishing, 2019, 384(1): 012191.

[40] Rezvani Tavakol M, Yarmohammad Tooski M, Jabbari M, et al. Effect of graphene nanoparticles on the strength of sandwich structure inspired by dragonfly wings under low-velocity impact[J]. Polymer Composites, 2021, 42(10): 52495264.

[41] Chen M, Qu D H, Tian H. Dragonflywinginspired polymer design for property enhancement[J]. Matter, 2021, 4(8): 26742676.

[42] Sudo S, Takagi K, Tsuyuki K, et al. Dynamic behavior of dragonfly wings[J]. Journal of the Japanese Society for Experimental Mechanics, 2008, 8(Special_Issue): s163s168.

[43] Cheeseman S, Owen S, Truong VK, Meyer D, Ng SH, Vongsvivut J, Linklater D, Tobin MJ, Werner M, Baulin VA, Luque P, Marchant R, Juodkazis S, Crawford RJ, Ivanova EP. Pillars of Life: Is There a Relationship between Lifestyle Factors and the Surface Characteristics of Dragonfly Wings? ACS Omega. 2018 Jun 30;3(6):60396046. doi: 10.1021/acsomega.8b00776. Epub 2018 Jun 5. PMID: 30221231; PMCID: PMC6130794.

[44] Arjangpay A, Darvizeh A, Tooski M Y. Effects of structural characteristics of a bionic dragonfly wing on its low velocity impact resistance[J]. Journal of Bionic Engineering, 2018, 15(5): 859871.

[45] Ho W H, New T H, Matare E. Unsteady CFD analysis of an oscillating Aerofoil inspired by dragonfly wings[J]. Proceedings of Topical Problems of Fluid Mechanics, 2017: 150166.

[46] Xu J H, Liu T, Zhang Y, et al. Dragonfly winginspired architecture makes a stiff yet tough healable material[J]. Matter, 2021, 4(7): 24742489.

[47] Kawabe H, Aoki Y, Sugimoto S, et al. Application of Macroscopic Structures on Dragonfly Wings to an Aircraft Design Approach[C]//AIAA AVIATION 2020 FORUM. 2020: 2664.

[48] Huixiang L, Guoyi H, Qi W. Numerical study on the aerodynamic performance of theflexible and corrugated forewing of dragonfly in gildingflight[J]. Journal of Mechanics, 2019, 51(1): 94102.

[49] Lee M. Dragonfly wings: special structures for aerial acrobatics[M]//Remarkable Natural Material Surfaces and Their Engineering Potential. Springer, Cham, 2014: 6577.

[50] Zhang, Y., Jiang, L., Zhou, W. et al. Dynamic response analysis of a multiplebeam structure subjected to a moving load. Earthq. Eng. Eng. Vib. 21, 769–784 (2022). /doi.org/10.1007/s1180302221063.

[51] Moravyík L', Vincúr R, Rózová Z. Analysis of the Static Behavior of a Single Tree on a Finite Element Model. Plants (Basel). 2021 Jun 24;10(7):1284. doi: 10.3390/plants10071284. PMID: 34202797; PMCID: PMC8309158.

[52] Holmes J D. Effective static load distributions in wind engineering[J]. Journal of wind engineering and industrial aerodynamics, 2002, 90(2): 91109.

[53] Korunoviæ L M, Milanoviæ J V, Djokic S Z, et al. Recommended parameter values and ranges of most frequently used static load models[J]. IEEE Transactions on Power Systems, 2018, 33(6): 59235934.
[54] Yu Y, Pu G, Jiang T, et al. A dragonfly wing inspired biomimetic aerodynamic thrust bearing for increased load capacity[J]. International Journal of Mechanical Sciences, 2020, 176: 105550.
[55] Zhao Y, Yang H, Wang D, et al. Reconstruction of bionic models and nanomechanical behavior of dragonfly membranous wings[J]. International Journal of Modern Physics B, 2022: 2250084.
[56] Magnucki K, Lewinski J, Cichy R. Bending of beams with bisymmetrical cross sections under nonuniformly distributed load: analytical and numericalFEM studies[J]. Archive of Applied Mechanics, 2019, 89(10): 21032114.
[57] Zheng H, Hablicsek M, Akbarzadeh M. Lightweight structures and the geometric equilibrium in dragonfly wings[C]//Proceedings of IASS Annual Symposia. International Association for Shell and Spatial Structures (IASS), 2020, 2020(14): 112.
[58] Guillerm V, Eddaoudi M. The importance of highly connected building units in reticular chemistry: Thoughtful design of metal–organic frameworks[J]. Accounts of Chemical Research, 2021, 54(17): 32983312.
[59] Li Z X. Structure Mechanics analysis with different Construction Schemes in largespan space Grid structure[C]//Advanced Materials Research. Trans Tech Publications Ltd, 2013, 788: 534537.
[60] Jigang Z, Tongbo Z, Jinping O U. Reliability and seismic analyses of the grid structure for swimming and diving hall in Qingdao sports center[J]. Engineering Mechanics, 2010, 27(Supplement I): 260265.
[61] Medl A, Mayr S, Rauch H P, et al. Microclimatic conditions of 'Green Walls', a new restoration technique for steep slopes based on a steel grid construction[J]. Ecological engineering, 2017, 101: 3945.
[62] Hajovsky R, Pies M, Velicka J. Monitoring the condition of the protective fence above the railway track[J]. IFACPapersOnLine, 2019, 52(27): 145150.
[63] Wang X, Burghardt D. A meshbased typification method for building groups with grid patterns[J]. ISPRS International Journal of GeoInformation, 2019, 8(4): 168.
[64] Saito Y, Watada R, Oshima T, et al. A Showroom with a Mesh Structure in Roppongi, Tokyo: Design and Construction[C]//Proceedings of IASS Annual Symposia. International Association for Shell and Spatial Structures (IASS), 2019, 2019(22): 18.

Biographies

Yangyang Wei, 2012–2014, he received his Master's degree in Industrial Engineering from Nanchang University. 2018 to 2021, he received his PhD in Data Science from the City University of Macau. In September 2021, he took up a position at the School of Architecture and Design at Nanchang University. His research interests include the areas of digital media technology, engineering education, computer-aided design, and architectural technology.

Huidi Guo, is currently a student at the School of Architecture and Design, Nanchang University. Her main research areas include graphic image processing, digital media technology, data visualisation design, information visualisation design, digital modelling and digital simulation.

Siyi Zhang, is currently a master's student in Architecture at the School of Architecture and Design, Nanchang University. His main research areas include modern architectural design, sustainable architecture, building physical environment simulation (fluid dynamics direction) and architectural heritage conservation.

Jingyuan Li, is currently a Master's student in Industrial Design Engineering at the School of Architecture and Design, Nanchang University. Her main research areas include industrial product design, sustainable product design, green material design, computer-aided design, and computer 3D modelling and analysis.

Yihan Wang, received her Master's degree in Industrial Design and Engineering from Nanchang University in 2013. From 2018 to 2022, she received her PhD in Urban Planning and Design from the City University of Macau. She is currently working in the Jiangxi Science and Technology Normal University. Her main research areas include intelligent engineering, urban planning, modern engineering education, and green architecture.

Chajuan Liu, is currently studying for a master's degree in the School of Architecture and Design, Nanchang University. Her research interests include structural mechanics, environmental design, urban planning and sustainable development.